Earth and Planetary Science Letters 473 (2017) 83–93

Contents lists available at ScienceDirect

Earth and Planetary Science Letters

www.elsevier.com/locate/epsl

Double-ramp on the Main Himalayan Thrust revealed by broadband waveform modeling of the 2015 Gorkha earthquake sequence

Xin Wang [a], Shengji Wei [a,b,*], Wenbo Wu [c]

[a] Earth Observatory of Singapore, Nanyang Technological University, Singapore
[b] Asian School of the Environment, Nanyang Technological University, Singapore
[c] Department of Geosciences, Princeton University, United States

ARTICLE INFO

Article history:
Received 15 March 2017
Received in revised form 16 May 2017
Accepted 22 May 2017
Editor: P. Shearer

Keywords:
2015 Gorkha earthquake
waveform modeling
focal mechanism
Main Himalaya Thrust
fault geometry

ABSTRACT

The 2015 M_w 7.8 Gorkha earthquake sequence that unzipped the lower edge of the Main Himalayan Thrust (MHT) in central Nepal provides an exceptional opportunity to understand the fault geometry in this region. However, the limited number of focal mechanisms and the poor horizontal locations and depths of earthquakes in the global catalog impede us from clearly imaging the ruptured MHT. In this study, we generalized the Amplitude Amplification Factor (AAF) method to teleseismic distance that allows us to model the teleseismic P-waves up to 1.5 Hz. We used well-constrained medium-sized earthquakes to establish AAF corrections for teleseismic stations that were later used to invert the high-frequency waveforms of other nearby events. This new approach enables us to invert the focal mechanisms of some early aftershocks, which is challenging by using other long-period methods. With this method, we obtained 12 focal mechanisms more than that in the GCMT catalog. We also modeled the high-frequency teleseismic P-waves and the surface reflection phases (pP and sP) to precisely constrain the depths of the earthquakes. Our results indicate that the uncertainty of the depth estimation is as small as 1–2 km. Finally, we refined the horizontal locations of these aftershocks using carefully hand-picked arrivals. The refined aftershock mechanisms and locations delineate a clear double-ramp geometry of the MHT, with an almost flat décollement sandwiched in between. The flat (dip ~7 degrees) portion of the MHT is consistent with the coseismic rupture of the mainshock, which has a well-constrained slip distribution. The fault morphology suggests that the ramps, both along the up-dip and down-dip directions, play a significant role in stopping the rupture of the 2015 Gorkha earthquake. Our method can be applied to general subduction zone earthquakes and fault geometry studies.

1. Introduction

Precise fault geometry is the key to understanding fault segmentation, which plays a crucial role in the initiation, propagation and termination of earthquakes, as well as in orogenic processes (Cattin and Avouac, 2000; Wesnousky, 2006; Avouac, 2007; Elliott et al., 2016; Hubbard et al., 2016; Qiu et al., 2016). The Main Himalayan Thrust (MHT) that has hosted a series of damaging earthquakes, and is the location of the highest mountain range in the world, has become the testing ground for fault geometry research (Fig. 1). Previous studies have investigated the geometry of the MHT in central Nepal through receiver functions (Schulte-Pelkum et al., 2005; Nabelek et al., 2009; Duputel et al., 2016), structure geology (Pearson and DeCelles, 2005; Avouac, 2007; Hubbard et al., 2016), electronic and magnetic surveys (Lemonnier et al., 1999), seismicity (Pandey et al., 1995) and geodetic data (Elliott et al., 2016). Most of these studies share a common feature: the MHT is almost flat beneath the Lesser Himalaya, as a décollement that connects the Main Boundary Thrust (MBT) and the Main Frontal Thrust (MFT) at the surface, extends southwards in the Sub-Himalaya and steepens northwards in the Higher Himalaya, usually through a ramp (Avouac, 2007). However, there are large variations between the dimensions, depths and dips of these fault geometries, e.g. the size of the ramp and whether or not existence of other ramps beneath the Kathmandu Valley (Elliott et al., 2016; Hubbard et al., 2016).

Earthquakes are direct evidence of active faults: precise earthquake location and mechanism can provide vital information to infer the fault geometry of the MHT, where a series of large earthquakes took place (Sapkota et al., 2013; Hayes et al., 2015; Bollinger et al., 2016). However, the number of large earthquakes

* Corresponding author at: Earth Observatory of Singapore, Nanyang Technological University, 50 Nanyang Avenue, N2-01a-14, 639798, Singapore.
E-mail address: shjwei@ntu.edu.sg (S. Wei).

http://dx.doi.org/10.1016/j.epsl.2017.05.032

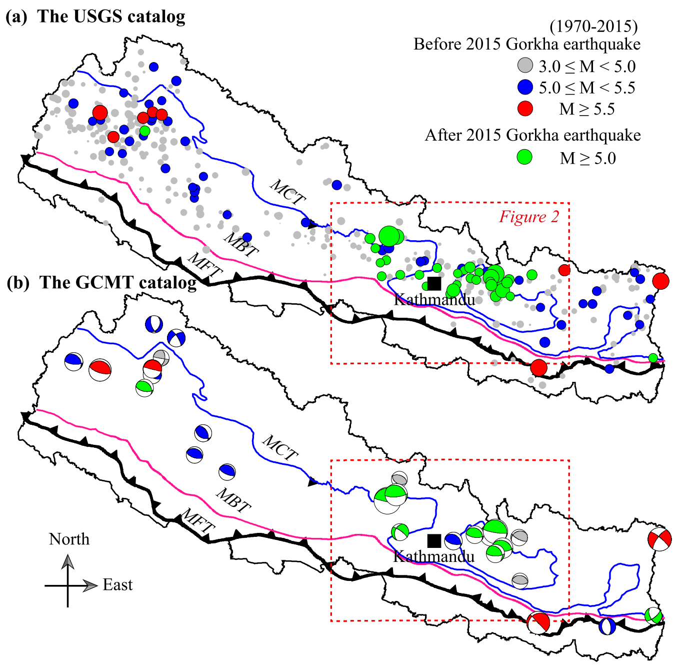

Fig. 1. (a) Earthquakes from the USGS catalog 1970–2016 (https://www.usgs.gov), with events of $M < 5.0$, $5.0 \leq M < 5.5$ and $M \geq 5.5$ before the 2015 Gorkha earthquake colored in gray, blue and red, respectively. Earthquakes with $M \geq 5.0$ after the 2015 Gorkha mainshock (including the mainshock) are colored in green. Main Frontal Thrust (MFT), Main boundary Thrust (MBT) and Main Central Thrust (MCT) are shown as black, pink and blue lines, respectively. (b) Earthquakes from the GCMT catalog 1976–2016 (http://www.globalcmt.org). Note the difference in sizable events before and after the 2015 Gorkha earthquake. (For interpretation of the colors in this figure, the reader is referred to the web version of this article.)

in Nepal that have modern broadband seismic records is very limited: between the 1970 and 2015 Gorkha earthquake, only 8 events with magnitude larger than 5.5 occurred in the entire country (Fig. 1). The source parameters (location, mechanism, rupture extents) for earthquakes that occurred before the era of modern seismic instruments have been poorly constrained. The large uncertainties of source parameters and lack of modern seismicity have impeded us from inferring the structure of faulting from these historical earthquakes.

The 2015 Gorkha earthquake sequence that unzipped the lower edge of the MHT in central Nepal provides an exceptional opportunity to better understand the fault geometry in this region (Fig. 2), as the number of sizable earthquakes (33 events with $M > 5.0$) in this sequence is comparable to the sum of events that occurred from 1970 to 2015 (before the Gorkha earthquake) (Fig. 1). However, only 9 of these 33 events—including the mainshock and two aftershocks with normal focal mechanisms—have Global Centroid Moment Tensor (GCMT) solutions (Fig. 1). This is because most of the aftershocks occurred immediately after the mainshock and the M_W 7.2 aftershock, and therefore the long-period seismic signals produced by the aftershocks were contaminated by the surface waves or the coda from the mainshock or previous large event (Fig. 3). In addition, the depths are relatively poorly constrained in the GCMT solutions—similar to other long-period solutions for shallow events. Thus, it is difficult to use the limited number of events with poor locations to delineate the fault geometry of the MHT. Although the Gorkha seismicity has been relocated by various studies using either local and/or teleseismic arrival time data (Adhikari et al., 2015; Bai et al., 2016), the depths and horizontal locations of earthquakes among these catalogs still vary significantly (Fig. 4 and Fig. S8). All these factors obstruct our understanding of the geometry of the MHT using seismicity.

To overcome these difficulties, we generalized the Amplitude Amplification Factor (AAF) method to teleseismic distance that allows us to determine the focal mechanisms of a portion of early aftershocks with high-frequency teleseismic P-waves, which resulted in a dozen more solutions than those found in available catalogs. We then modeled the high-frequency teleseismic depth phases to precisely determine the depth of these events; we also further relocated the horizontal position of these events using carefully hand-picked P-wave arrival times. The refined earthquake catalog illuminates a clear MHT that shows double ramps with the coseismic slip of the mainshock sandwiched in between. In this paper, we will describe the data and approaches used in greater detail, followed by the results; we will then discuss the implications of our findings.

2. Focal mechanism inversion for early aftershocks

Our approach in resolving the focal mechanism of more aftershocks benefits from the usage of high-frequency ($0.5 \sim 1.5$ Hz) teleseismic P-waves. At this frequency range, the signal-to-noise-ratio (SNR) of P-waves is usually higher than that at longer periods, particularly for some early aftershocks (Fig. 3), because the signals from the previous earthquakes are attenuated more and the ambient noise level is usually lower. However, to use the waveform for inversion at this frequency range, we also cannot ignore the site condition and structure complexity along the ray path. To deal with this challenge, we took advantage of earthquakes that have reliable long-period focal mechanism solutions to establish path calibration. We established this calibration by fixing the focal mechanism to the long-period solution and predicting the teleseismic P-waves at high-frequency ranges. We found that, at $0.5 \sim 1.5$ Hz, the shape of first 3 s of teleseismic P-waves can still be well-fitted by the 1D synthetics with an amplitude amplification factor (AAF) applied to the synthetics to correct for the imperfect green's functions (Fig. S1, S5). A similar approach has been successfully applied to the small earthquake focal mechanism inversion, using regional waveform data in Southern California (Tan and Helmberger, 2007). The key here is to find the calibration events that have reliable long-period focal mechanism solutions. To ensure the rupture complexity of calibration events can be ignored at 0.5–1.5 Hz, ideally we need to select earthquakes with source durations less than about ~0.6 s, so that they can be considered as point sources. Longer source duration will produce a roughly constant shift to all the AAFs. Our tests indicate that the contribution to the standard deviation (see supplement materials for more details) using a 1.5 s source time function is about 0.2 (Fig. S4), which is the threshold we used in this study. It is also important to note that a stable and reliable long-period focal mechanism solution is required for the calibration events. Using these criteria, we found two aftershocks (2015/04/26 16:26 (UTC) M_W 5.0 and 2015/05/16 13:34 (UTC) M_W 5.2) in the 2015 Gorkha earthquake sequence that can be used as calibration events.

Although there are reported moment tensor solutions (e.g., GCMT, W-phase) for these calibration events and some other large aftershocks, we still wanted to have our own solutions, in particular for depth, which reveal large variations among different catalogs (Fig. 4). Here we used extended teleseismic P and SH waves, which contain the depth phases (e.g. pP, sP, sS) that are most sensitive to the focal depth to invert the focal mechanism and depth. Many practices have demonstrated that teleseismic P and SH waves are less affected by the 3D velocity structure and can result in higher resolution in fault plane solutions, since most of the ray paths lie in the relatively simple mantle (Zhan et al., 2012). Given that we are using a 1D velocity model in the inversion (as in most moment tenor inversion methods), and that